Impedance analysis of renal vascular smooth muscle cells

Lavanya Balasubramanian, Kay-Pong Yip, Tai-Hsin Hsu and Chun-Min Lo

Am J Physiol Cell Physiol 295:954-965, 2008. First published Aug 6, 2008;
doi:10.1152/ajpcell.00009.2008

Am J Physiol Cell Physiol 295: C954–C965, 2008.
First published August 6, 2008; doi:10.1152/ajpcell.00009.2008.

Impedance analysis of renal vascular smooth muscle cells

Lavanya Balasubramanian,[1] Kay-Pong Yip,[1] Tai-Hsin Hsu,[3] and Chun-Min Lo[2]

[1]*Department of Molecular Pharmacology and Physiology and* [2]*Department of Physics, University of South Florida, Tampa, Florida; and* [3]*Department of Physics, National Cheng Kung University, Tainan, Taiwan*

Submitted 8 January 2008; accepted in final form 31 July 2008

Balasubramanian L, Yip K-P, Hsu T-H, Lo C-M. Impedance analysis of renal vascular smooth muscle cells. *Am J Physiol Cell Physiol* 295: C954–C965, 2008. First published August 6, 2008; doi:10.1152/ajpcell.00009.2008.—Impedance of renal vascular smooth muscle cells (VSMCs) cultured on microelectrodes was measured by electric cell-substrate impedance sensing. Changes in measured impedance as a function of frequency were compared with the calculated values obtained from an extended cell-electrode model to estimate the junctional resistance, distance between the ventral cell surface and the substratum, and apical and basolateral membrane capacitances of renal VSMCs. This cell-electrode model was derived to accommodate the slender and rectangular shape of VSMCs. The calculated changes in impedance (Z_{cal}) based on the model agreed well with the experimental measurement (Z_{exp}), and the percentage error defined as $|(Z_{cal} - Z_{exp})/Z_{exp}|$ was 1.0%. To test the sensitivity of the new model for capturing changes in cell-cell and cell-substrate interactions induced by changes in cellular environment, we then applied this model to analyze timpedance changes induced by an integrin binding peptide in renal VSMCs. Our result demonstrates that integrin binding peptide decreases junctional resistance between cells, increases the distance between the basolateral cell surface and substratum, and increases the apical membrane capacitance, whereas the basolateral membrane capacitance stays relatively stable. This model provides a generic approach for impedance analysis of cell layers composed of slender, rectangular cells.

electric cell-substrate impedance sensing; cell attachment; cell adhesion; extracellular matrix; integrin

MICROELECTRODE ARRAYS PROVIDE a simple interface for monitoring impedance characteristics of populations of cultured cells over extended periods. The cell-electrode interface is created as cells attach directly to planar electrode structures. Since cell membranes exhibit dielectric properties, culturing cells over electrode surfaces will result in changes in the effective electrode impedance. Impedance measurements using alternate current (AC) techniques are based on the fact that intact living cells are excellent electrical insulators at low signal frequencies, hence a noninvasive assay of morphological properties of cultured cells. Impedance measurement using microelectrodes was first used to study the characteristics of anchorage-dependent cultured cell lines by Giaever and Keese (6, 8). A cell-based biosensor, referred to as electric cell-substrate impedance sensing (ECIS), was developed by them and can be applied to quantify cell behavior in tissue culture (5, 7). By culturing cells on small gold film electrodes and monitoring impedance changes caused by adherent cells, one can quantify changes in the capacitance of the cell membrane, cell-substrate separation, and cell-cell separation with exquisite sensitivity and in a noninvasive manner (5, 15, 17). More importantly, the cell-cell and cell-substrate interactions are always associated with frequency-dependent changes in impedance. Because cell-cell and cell-substrate interactions are sensitive to drugs, toxins, and other chemicals, cell-cell and cell-substrate interactions measured by ECIS can be used as an index to represent the overall cell response resulting from the changes in the cellular environment. We have applied ECIS to quantify changes in cell-cell and cell-substrate separation in response to environmental stimuli such as temperature, glucose deprivation, pH variation, Ca^{2+} removal, and mechanical stress (16–19). Furthermore, this emerging technique has been extended for monitoring cellular responses to toxic or noxious agents such as cytochalasin D, prostaglandin E_2, detergents, cadmium chloride, and bacterial proteins that perturb extracellular matrix and cytoskeleton (12–14, 24, 28, 29). In these studies, a dose-dependent relationship was generally observed and was highly reproducible.

Previously, there have been two cell-electrode models used for impedance analysis of the frequency scan data obtained by ECIS. One is appropriate for cells with disklike shape, such as transformed fibroblasts, endothelial cells, and epithelial cells (3, 5, 17), and the other is used for rectangular cells with semicircular ends, such as normal fibroblasts (15). By fitting the experimental data into the model with nonlinear least-squares fitting, we have been able to estimate three morphological parameters from fibroblasts, namely, R_b, α, and C_m. R_b is the junctional resistance between cells, C_m is the transcellular membrane capacitance representing a series connection of both basolateral and apical membranes, and α is equal to $0.5W(\rho/h)^{1/2}$, where W is the cell width, ρ is the resistivity of the solution, and h is the average separation distance between the cells and the substratum (see *Glossary*).

Cell-cell and cell-substrate interactions are essential determinants in cell migration, embryonic development, and tissue formation. With an emerging interest to delineate the mechanisms of cell-cell and cell-substrate interactions in response to environmental stimuli using ECIS, the selection of an appropriate cell-electrode model for fitting the experimental data is critical. In this article, we have modified the previous rectangular model by accommodating the slender and rectangular shape of vascular smooth muscle cells (VSMCs) and have extended the model so that apical membrane capacitance (C_a) and basolateral membrane capacitance (C_b) can be estimated separately. Our previous rectangular model does not include the difference of current distribution through basolateral and apical membranes. In this more comprehensive model, we assume that the electrical potential inside the cell, V_i, is independent of the position inside the cell. Therefore, although

Address for reprint requests and other correspondence: C.-M. Lo, Dept. of Physics, College of Arts and Sciences, Univ. of South Florida, 4202 East Fowler Ave., PHY303, Tampa, FL 33620-5700 (e-mail: cmlo@cas.usf.edu).

The costs of publication of this article were defrayed in part by the payment of page charges. The article must therefore be hereby marked "*advertisement*" in accordance with 18 U.S.C. Section 1734 solely to indicate this fact.

the transcellular current entering through the basolateral membrane decreases, as its position moves away from the symmetrical center of the basolateral cell surface, the transcellular current exiting through the apical membrane is uniform. Since the apical cell surface of an adherent cell usually has more membrane folding than the basolateral membrane, the apical membrane capacitance should be different from that of the basolateral membrane.

We selected VSMCs from renal vasculature to test our model (4). The experimental impedance data and the data calculated by the model were consistently agreeable at various frequencies from 25 to 60 kHz. We were able to measure R_b, h, C_a, and C_b in VSMCs. To further verify this new model for impedance analysis, we tested the hypothesis that the integrin binding hexapeptide GRGDSP (Gly-Arg-Gly-Asp-Ser-Pro) induces morphological changes in VSMCs that can be detected through continuous analysis of ECIS data output. The results demonstrate that integrin binding peptide decreases junctional resistance between cells, increases the distance between the basolateral cell surface and substrate, and increases the apical membrane capacitance, indicating the occurrence of cell contractile activity. Thus we describe a comprehensive cell-electrode model that may serve as a new approach for impedance analysis of cell layers with long rectangular cell shape in general.

Glossary

C_a Specific capacitance of the apical cell membrane ($\mu F/cm^2$)
C_b Specific capacitance of the basolateral cell membrane ($\mu F/cm^2$)
C_n Measured capacitance of the cell-free electrode ($\mu F/cm^2$)
f Frequency of the AC signal (Hz)
h Average separation distance between basolateral cell surface and substratum (nm)
I_c Total current across the cell-covered electrode (A)
I_{ct} Total current through the area of a single cell (A)
I_i Transcellular current through the apical cell surface (A)
L Cell length (μm)
N Number of cells on the electrode
R_b Junctional resistance between adjacent cells over a unit cell area ($\Omega \cdot cm^2$)
R_m Specific resistance of the cell membrane ($\Omega \cdot cm^2$)
R_n Measured resistance of the cell-free electrode ($\Omega \cdot cm^2$)
S Electrode area (cm^2)
V_c Applied voltage across the cell-electrode system (V)
V_i Electrical potential inside the cell (V)
V_s Electrical potential in solution on the dorsal side of the cells (V)
W Cell width (μm)
Z_a Specific impedance through the apical cell membrane ($\Omega \cdot cm^2$)
Z_b Specific impedance through the basolateral cell membrane ($\Omega \cdot cm^2$)
Z_c Specific impedance of the cell-covered electrode ($\Omega \cdot cm^2$)
Z_n Specific impedance (impedance for a unit area) of the cell-free electrode ($\Omega \cdot cm^2$)
ρ Resistivity of the cell culture medium ($\Omega \cdot cm$)

MATERIALS AND METHODS

Isolation of renal VSMCs. All experiments were performed under protocols approved by the University of South Florida's Animal Care and Use Committee. Kidneys and renal arterioles were harvested from male Sprague-Dawley rats. Renal VSMCs were isolated with enzyme digestion from dissected arcuate arteries and cortical radial arteries (9). The arteries were first digested with papain and then digested with 2% collagenase type 4, 1% trypsin inhibitor, and 0.5% elastase. All digestions were performed in low-calcium dissociation solution at 37°C. The vessels were then triturated, and VSMCs were collected into glass-bottomed petri dishes coated with Matrigel (BD Bioscience).

Impedance measurement of cell attachment. Electrode arrays, relay bank, lock-in amplifier, and software for the ECIS measurement were obtained from Applied BioPhysics (Troy, NY). Each electrode array consists of eight wells that are 1 cm in height and 0.8 cm^2 in bottom area; each well contains a 250-μm-diameter gold electrode (area $\sim 5 \times 10^{-4}$ cm^2) and a much larger gold counter electrode. The large electrode and one of the small electrodes were connected via the relay bank to a phase-sensitive lock-in amplifier, and AC was applied to the sample through a 1-MΩ resistor. Experimental setup and circuit connection were that same as we previously described (17). For cell attachment and spreading assay, VSMCs were plated into electrode wells at a density of 10^5 cells/cm^2, and impedance changes were measured immediately. For impedance measurements of VSMC monolayers upon addition of GRGDSP, Ham's F12 medium supplemented with 10% fetal bovine serum (FBS; 0.4 ml) was added over the electrode in each well. Cells were allowed to attach and spread for at least 24 h before impedance was measured. After 24 h in culture, the confluency and viability of the cell monolayer were confirmed by light microscopy and electrically by measuring the resistance values. Attached cells on the electrode acted as insulating particles, and the main current must therefore pass around the cells. The changes in cell dimensions manifested as changes in impedance while the cell-covered area and/or the cell-substrate separation changed. Hexapeptide GRGDSP or GRGESP (Gly-Arg-Gly-Glu-Ser-Pro) in Hanks' balanced salt solution (HBSS; Cellgro; pH 7.1~7.4) or HBSS alone was added to each cell-covered electrode well. The electrical impedance of each well was measured every 2 min. We applied a 1-V AC signal at 4 or 40 kHz to the sample through a 1-MΩ resistor to maintain a constant current of 1 μA through the sample. By analogy with Ohm's law for DC circuits, $Z = V/I = R - j(1/\omega C)$, the equivalent resistance and capacitive reactance of the sample were calculated by dividing the measured in-phase and out-of-phase voltages by 1 μA, respectively. Typically, the magnitude of the in-phase voltage drop across the cell-free electrode was in the order of a millivolt and increased to several millivolts with a confluent VSMC layer grown on the top. The resultant voltage drop of a few millivolts had no detectable effect on the cells; hence, the measurement is believed to be noninvasive (18, 26).

Impedance measurement of cell morphology. Frequency scan is another main method in ECIS with which we can measure the impedance of the cell-electrode system as a function of frequency ranging from 25 to 60 kHz. It took ~2.5 min to measure each electrode. Generally, to obtain impedances as a function of frequency for both a cell-free electrode and the same electrode covered with confluent cells, we applied frequency scan before and after cells attached to the electrode. By comparing the experimental data of confluent cell monolayers with the calculated values obtained from the cell-electrode model, frequency scan measurements can provide morphological parameters such as R_b and h (5, 15, 17). To obtain the best-fitting values, first the model parameters R_b, α, C_a, and C_b were arbitrarily

chosen to get calculated resistance and capacitive reactance using the cell-electrode model described in this article. The deviation or error between the calculated (Z_{cal}) and measured impedance (Z_{exp}) data was defined by $|Z_{cal} - Z_{exp}|$. Our curve-fitting criterion, know as the nonlinear least-squares fitting, was that the sum of the square of the errors was a minimum. Since both resistance and capacitive reactance at 23 different frequencies were considered equally important for data fitting, there were a total of 46 errors included in the sum. By using matrix algebra, model parameters were changed, and this process was repeated by refining the parameters until the final minimum was determined.

Model derivation. The primary objective of an ECIS model is to calculate the specific impedance of a cell-covered electrode as a function of frequency, Z_c, from the measured values of a cell-free electrode, Z_n, with only a few cellular morphological parameters, which are specific to different cell types and can be used as an index to examine the cell-cell and cell-substratum interaction. After the measured impedance data of the same electrode covered with cells are fitted with the calculated values of Z_c, those cellular morphological parameters can then be determined. The various current paths are sketched in Fig. 1. To make the calculations tractable, six simplifying assumptions must be made: *1*) the cells have a rectangular shape with length L and width W; *2*) the current one-dimensionally and symmetrically passes from the central line to the edges of the cell through the space formed between the ventral surface of the cell and the substratum; *3*) the current density under the cells does not change in the vertical direction; *4*) the electrode potential V_c is a constant independent of position, *5*) the potential in solution on the dorsal side of the cells is likewise treated as a constant V_s (for convenience, we set $V_s = 0$; this assignment does not affect the calculated impedance); and *6*) the electrical potential inside the cell V_i, although a function of V_c, is independent of position inside the cell.

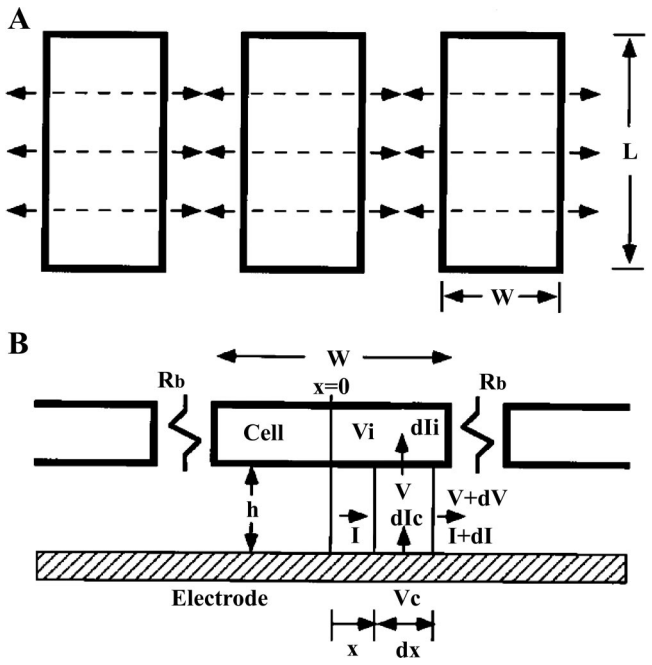

Fig. 1. A schematic diagram of the cell-electrode model for cell layers cultured on a gold electrode. Cells are considered as a flat rectangular ($L \times W$) box. *A*: top view of the cell layer, where in the channel spaces between the cell and the substratum, currents coming from the electrode one-dimensionally and symmetrically pass to the edges of the cell and then through the paracellular space between cells. *B*: side view of the cell layer emphasizing the cell-substrate spaces and the various current paths. The side view diagram is useful in constructing the *Eqs. 1–4* and *12–15*. The increased impedance of a cell-covered electrode is largely due to the current under the cells and comes in addition to the transcellular and paracellular pathways. See *Glossary* for definition of variables.

From the definition of the impedance of an AC circuit, Z_c = (electrode area) (V_c/I_c), where I_c is the total current across the cell-covered electrode. Because confluent cells form a monolayer on the electrode, if the number of cells on the electrode is N, electrode area = $N \times$ cell area = NLW and $I_c = NI_{ct}$. I_{ct} is the total current through the area of a single cell. Therefore, as long as I_{ct} can be calculated as a function of the applied voltage across the cell-electrode system, V_c, the value for Z_c can be solved by the equation $Z_c = LWV_c/I_{ct}$. From Fig. 1 and Ohm's law for AC circuits, we get

$$-\frac{dV}{dx} = \frac{\rho}{hL}I, \tag{1}$$

$$V_c - V = \frac{Z_n}{L}\frac{dI_c}{dx}, \tag{2}$$

$$V - V_i = \frac{Z_b}{L}\frac{dI_i}{dx}, \tag{3}$$

and

$$\frac{dI}{dx} = \frac{dI_c}{dx} - \frac{dI_i}{dx}. \tag{4}$$

Equations 1–4 can be combined to yield the following differential equation:

$$\frac{d^2V}{dx^2} - \gamma^2 V + \beta = 0, \tag{5}$$

where

$$\gamma^2 = \frac{\rho}{h}\left(\frac{1}{Z_n} + \frac{1}{Z_b}\right), \tag{6}$$

and

$$\beta = \frac{\rho}{h}\left(\frac{V_c}{Z_n} + \frac{V_i}{Z_b}\right). \tag{7}$$

The general solution of *Eq. 5* is

$$V = Ae^{\gamma x} + Be^{-\gamma x} + \frac{\beta}{\gamma^2}. \tag{8}$$

Putting *Eq. 8* into *Eq. 1*, with a boundary condition

$$I(x = 0) = 0, \tag{9}$$

we have $A = B$ and

$$I = \left(-\frac{hL}{\rho}\right)\gamma(Ae^{\gamma x} - Be^{-\gamma x}) = -\frac{2hLA}{\rho}\sinh(\gamma x). \tag{10}$$

Note that $\sinh(x) = (e^x - e^{-x})/2$ and $\cosh(x) = (e^x + e^{-x})/2$. The total current from the electrode area covered by a single cell is calculated as

$$I_{ct} = 2\int_0^{\frac{W}{2}} dI_c = \frac{2L}{Z_n}\int_0^{\frac{W}{2}}(V_c - V)dx = -\frac{4LA}{Z_n\gamma}\sinh\left(\frac{\gamma W}{2}\right) + \frac{LW}{Z_n + Z_b}(V_c - V_i), \tag{11}$$

where

$$\frac{\gamma W}{2} = \frac{W}{2}\left[\frac{\rho}{h}\left(\frac{1}{Z_n} + \frac{1}{Z_b}\right)\right]^{1/2} = \alpha\left(\frac{1}{Z_n} + \frac{1}{Z_b}\right)^{1/2}. \quad (12)$$

The transcellular current uniformly through the apical cell surface is calculated as

$$I_i = \frac{V_i LW}{Z_a}. \quad (13)$$

With two boundary conditions on current I, I_{ct}, and I_i (*Eqs. 10*, *11*, and *13*),

$$2I(x = W/2)\frac{R_b}{LW} = V(x = W/2), \quad (14)$$

and

$$I_{ct} = I_i + 2I(x = W/2), \quad (15)$$

we can determine the two constants A and V_i:

$$A = \frac{-\beta}{\gamma^2\left[2\cosh\left(\frac{\gamma W}{2}\right) + \frac{4R_b\gamma h}{\rho W}\sinh\left(\frac{\gamma W}{2}\right)\right]}, \quad (16)$$

and

$$\frac{V_i}{V_c} = \frac{1 - \frac{2}{\gamma W\coth\left(\frac{\gamma W}{2}\right) + 2R_b\left(\frac{1}{Z_n} + \frac{1}{Z_b}\right)}}{\frac{Z_a + Z_n + Z_b}{Z_a} + \frac{2Z_n}{Z_b\left[\gamma W\coth\left(\frac{\gamma W}{2}\right) + 2R_b\left(\frac{1}{Z_n} + \frac{1}{Z_b}\right)\right]}}. \quad (17)$$

By using *Eq. 11*, the specific impedance for a cell-covered electrode is expressed as

$$\frac{1}{Z_c} = \frac{I_{ct}}{V_c LW} = -\frac{4A}{V_c Z_n \gamma W}\sinh\left(\frac{\gamma W}{2}\right) + \frac{1}{(Z_n + Z_b)}\left(1 - \frac{V_i}{V_c}\right). \quad (18)$$

After putting the values of A (*Eq. 16*) into *Eq. 18*, the final result for Z_c can be solved in a closed form as

$$\frac{1}{Z_c} = \frac{1}{Z_n + Z_b}\left[1 - \frac{V_i}{V_c} + \frac{\frac{2Z_b}{Z_n} + \frac{2V_i}{V_c}}{\gamma W\coth\left(\frac{\gamma W}{2}\right) + 2R_b\left(\frac{1}{Z_n} + \frac{1}{Z_b}\right)}\right], \quad (19)$$

where V_i/V_c is given from *Eq. 17* as

$$Z_n = S\left(R_n + \frac{1}{i2\pi f C_n}\right), \quad (20)$$

$$Z_a = \left(\frac{1}{R_m} + i2\pi f C_a\right)^{-1}, \quad (21)$$

and

$$Z_b = \left(\frac{1}{R_m} + i2\pi f C_b\right)^{-1}. \quad (22)$$

where S is electrode area, which equals 5×10^{-4} cm^2, and f is frequency of the AC signal. R_n and C_n are measured resistance and capacitance of the cell-free electrode, respectively. R_m is specific resistance of the cell membrane, and C_a and C_b are specific capacitances of the apical and basolateral cell membranes, respectively. It has been recognized that the electrode-electrolyte interface has a capacitive imaginary component. Following tradition, we represent the specific impedance of the cell-free electrode, Z_n, as a series combination of a resistance (R_n) and a capacitance (C_n) as shown in *Eq. 20* (16, 22, 25). R_n and C_n are based on the in-phase and out-of-phase voltage data obtained from the lock-in amplifier at different frequencies. R_n and $(2\pi f C_n)^{-1}$ are respectively so-called resistance and capacitive reactance of the measured impedance of the cell-free electrode, Z_n. It should be noted that the Z_n value is frequency dependent, and so are R_n and C_n (22). We also assume that the specific resistance of the cell membrane, R_m, is 10^3 $\Omega\cdot$cm^2 and that the specific impedances of the apical and basal cell membranes, Z_a and Z_b, can be calculated as a resistor and a capacitor in parallel as shown in *Eqs. 21* and *22*. The frequency dependence does not appear explicitly in *Eq. 19*, since it is included in the impedances Z_n, Z_a, and Z_b. Together, using *Eq. 19* with V_i/V_c given by *Eq. 17*, the calculated values of Z_c over the measured frequency range are based on a set of parameters, specifically R_b, α, C_a, and C_b.

Now, if we characterize the cell body as basolateral and apical membranes packed together and assume that $C_a = C_b = C_m$ (16), the overall membrane impedance for the transcellular current to pass through is therefore

$$Z_m = 2\left(\frac{1}{R_m} + i2\pi f C_m\right)^{-1}. \quad (23)$$

In this special circumstance, since currents passing through basolateral and apical membranes are identical, *Eq. 3* can be rewritten as

$$V = \frac{Z_m}{Ld x}dI_i. \quad (24)$$

As before, *Eqs. 1*, *2*, *4*, and *24* can be combined to yield *Eq. 5*. With the same boundary conditions described in *Eqs. 9*, *14*, and *15*, the specific impedance for a cell-covered electrode can be solved in a closed form as

$$\frac{1}{Z_c} = \frac{1}{Z_n + Z_m}\left[1 + \frac{\frac{2Z_m}{Z_n}}{\gamma W\coth\left(\frac{\gamma W}{2}\right) + 2R_b\left(\frac{1}{Z_n} + \frac{1}{Z_m}\right)}\right]. \quad (25)$$

This simplified result is exactly the same as the solution obtained from the previous rectangular model, where the calculated values of Z_c are based on three parameters only: R_b, α, and C_m (15). As expected, *Eq. 25* can be easily obtained by putting $V_i = 0$ and $Z_b = Z_m$ into *Eq. 19*.

RESULTS

Measurement of cell attachment and spreading. Rates of cell attachment and spreading to microelectrodes are known to be dependent on the type of extracellular matrix (ECM) protein coated on the substratum (1, 2, 23, 26, 32). To examine the preference of the cultured VSMCs to various ECM proteins, we coated ECIS electrodes with fibronectin, vitronectin, laminin, bovine serum albumin (BSA), and collagen. Uncoated electrodes were used as negative control, where the adsorbed protein layer was simply a collection of those proteins found in the FBS used to supplement the growth medium. Figure 2 shows a typical result obtained from VSMCs using the ECIS attachment assay. The resistance data are presented as the measured resistance normalized to its value at the start of each run. In this case the cells were inoculated on the electrodes at *time 0*, and the impedances were monitored for 12 h using a 1-μA AC signal at 40 kHz. As shown in Fig. 2, the responses were different depending on the ECM coatings on ECIS electrodes. After the inoculation, the resistance of the fibronectin-coated electrode increased more rapidly with time compared with that of the other five electrodes. This initial quick

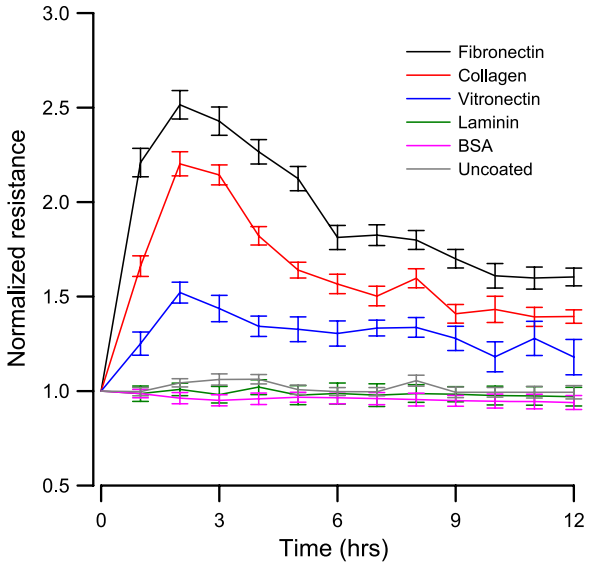

Fig. 2. Average normalized resistance measured at 40 kHz showing the attachment and spreading of renal VSMCs on different ECM proteins ($n = 4$ for each condition). Data points for each concentration were collected every 2 min for 12 h, but only points at 0, 1, 2, . . . , and 12 h were averaged and shown. The different coatings used are represented as fibronectin (black), collagen I (red), vitronectin (blue), laminin (green), bovine serum albumin (BSA; pink), and uncoated electrodes (gray).

rise in the curve was because suspended VSMCs continuously settled down, attached to the electrodes, and effectively blocked the area available for current. By the end of ~2 h, the resistance reached the peak and then started to fall as the cells started to develop focal adhesions, spread, and push each other to form a monolayer. By 6 h, the cells attached, spread, and reached equilibrium. Smaller changes in the cell-electrode interaction due to cell motions caused the impedance to fluctuate with time. Changes in resistance for collagen- and vitronectin-coated electrodes lagged somewhat behind those for the fibronectin-coated electrode. There was hardly any increase in resistance for the laminin-coated, BSA-coated, or uncoated electrode. These results are consistent with observations from other laboratories that smooth muscle cells prefer fibronectin, vitronectin, and type I collagen for attachment, spreading, and the formation of stable focal adhesions (10, 20, 30).

Model analysis and cellular parameters for VSMCs. An important feature of the use of ECIS systems to measure impedance is the frequency-dependent nature, which is always associated with cell-cell and cell-substrate interactions. In these frequency scan experiments, the impedances of the electrode wells were measured under different frequencies. In Fig. 3, *A* and *B*, respectively, show the measured resistance and capacitance of an electrode without (lines without symbols) and with VSMCs (line with symbols) and the calculated values of Z_c (filled circles and crosses), which are based on the specific impedance of the cell-free electrode, Z_n, and the model. Since the solution resistance (constriction or spreading resistance between the smaller sensing electrode and the larger counter electrode) is a significant part of the measured impedance, it must first be subtracted from the measured impedance to perform the calculations and then be added back for comparison with the experimental results (5, 17). The numerical value of the constriction resistance is simply equal to the asymptotic value at high frequency of the measured resistance for a cell-free electrode. As evidenced in Fig. 3, both measured resistance (R_n; *A*) and capacitance (C_n; *B*) of a cell-free electrode (lines without symbols) decreased as the applied AC frequency increased; however, they varied in different ways as cells attached and spread on the electrodes (lines with symbols). At the high-frequency range, when cells covered up some of the electrode area, the resistance increased and the capacitance decreased, because the cells impaired the movement of ions, resulting in less current coming out of the electrode. At low frequency, both resistance and capacitance did not change much even when there were cells on the electrode, because the impedance from the electrode-electrolyte interface dominated the measured impedance. Note that Fig. 3 is a log-log plot. For analyzing differences in impedance

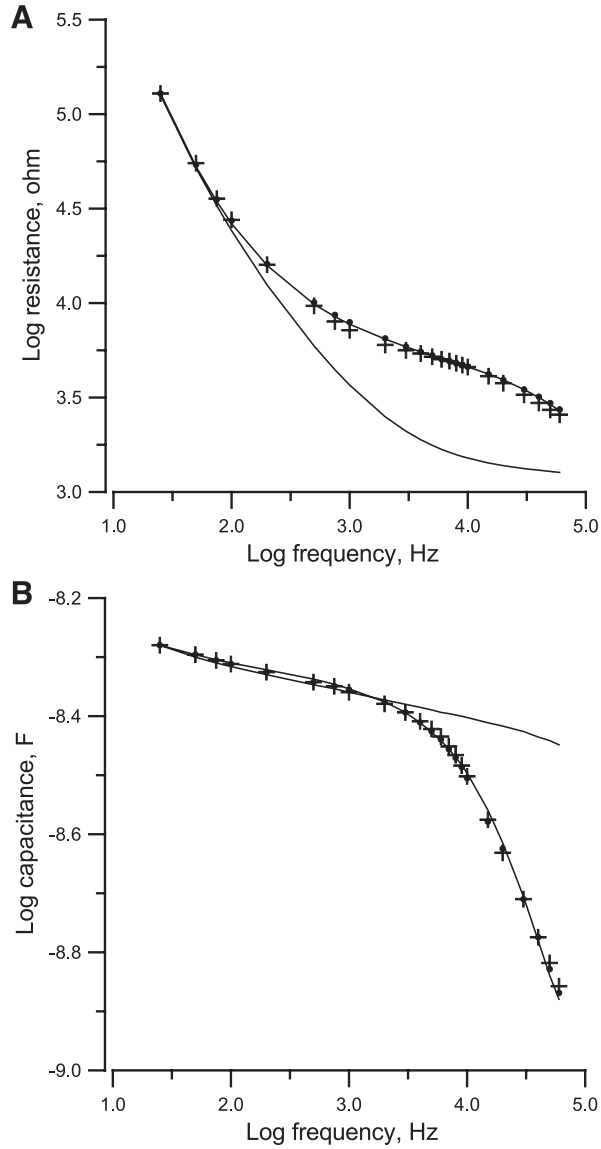

Fig. 3. Resistance (*A*) and capacitance (*B*) as a function of $\log_{10}$(frequency) obtained from a frequency scan measurement for a cell-free electrode (lines without symbols) and for the same electrode covered with a confluent monolayer of vascular smooth muscle cells (VSMCs; lines with symbols). Filled circles and crosses are calculated values based on the measured impedance of the cell-free electrode using *Eqs. 19* and *25*, respectively.

curves, it is helpful to use normalized values, where the impedance values from the electrode confluent with VSMCS are divided by the corresponding quantities for the cell-free electrode (Fig. 4). In general, the normalized resistance starts from 1.0 at 25 Hz, increases with increasing frequency to the highest value, ~3.1 at 6 kHz, and then decreases with increasing frequency until 2.1 at 60 kHz. The reason for the peak is that the constriction resistance masks the resistance of the cell-covered electrode at high frequency. Normalized capacitance, on the other hand, remains 1.0 from 25 Hz to 1 kHz and then decreases with increases in frequency until ~0.38 at 60 kHz.

We analyzed the measured impedance of the cell-covered electrode shown in Fig. 3 by using *Eq. 19* to determine R_b, α, C_a, and C_b. Both the resistive and reactive components of the measured impedance were fitted to the model equation by nonlinear least-squares fitting at 23 different frequencies ranging from 25 Hz to 60 kHz, allowing a precise determination of the model parameters. Cell length (L) and width (W) were estimated directly by phase-contrast microscopy, and for VSMCs their values were ~60 and 12 μm, respectively. With the least-squares method, the best-fitting values of R_b, α, C_a, and C_b for the data shown in Fig. 3 were 0.2 $\Omega\cdot cm^2$, 2.4 $\Omega^{1/2}\cdot cm$, 2.6 $\mu F/cm^2$, and 1.7 $\mu F/cm^2$. The average cell-substrate separation (h) was calculated from α by using *Eq. 11* with $\rho = 60\ \Omega\cdot cm$ and $W = 12\ \mu m$, and the result for h was 38 nm if $\alpha = 2.4\ \Omega^{1/2}\cdot cm$. The same measured impedance was also fitted by *Eq. 25* derived from the previous rectangular model (15), and the best-fitting values of R_b, α, and C_m were 0.2 $\Omega\cdot cm^2$, 2.5 $\Omega^{1/2}\cdot cm$, and 2.0 $\mu F/cm^2$. Along with the measured impedance data, the best-fitting curves achieved using *Eqs. 19* and *25* were normalized and are shown in Fig. 4. The measured impedance curve was better simulated by the calculated impedance curve derived from *Eq. 19* (filled dots) rather than by *Eq. 25* (crosses). Although both model equations resulted in similar fitting values of R_b and α, the minimum value of the root mean square of the errors (defined as $|Z_{cal} - Z_{exp}|$ in MATERIALS AND METHODS) was 452 Ω using *Eq. 19* and 572 Ω using *Eq. 25*. In addition, the average of the percentage error defined as $|(Z_{cal} - Z_{exp})/Z_{exp}|$ was 1.0% using *Eq. 19* and 2.3% using *Eq. 25*. Together, these results indicate that the curve fitting between calculated and experimental data was significantly improved by using *Eq. 19*.

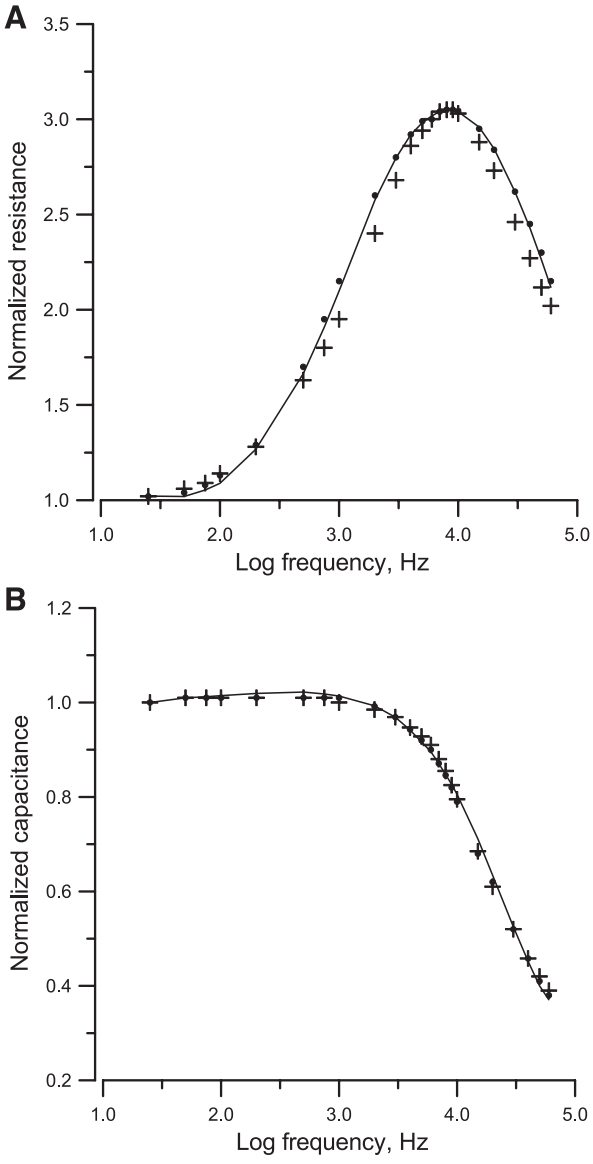

Fig. 4. Normalized resistance (*A*) and normalized capacitance (*B*) as a function of $\log_{10}$(frequency) for an electrode with a confluent VSMC layer. The curves were obtained from Fig. 3 by dividing the measured values for the cell-covered electrode by the corresponding values for the cell-free electrode. Again, the filled dots and crosses are calculated values using *Eqs. 19* and *25*, respectively.

We carried out a number of impedance measurements of confluent VSMC monolayers at 37°C and analyzed the data using both the previous and new rectangular models as well as the model based on disk-shaped cells (5). After the experimental data were fit individually using *Eq. 19*, the average values of R_b, h, C_a, and C_b were 0.32 ± 0.02 $\Omega\cdot cm^2$, 41 ± 0.3 nm, 2.6 ± 0.1 $\mu F/cm^2$, and 1.7 ± 0.1 $\mu F/cm^2$ ($n = 42$, Table 1). Compared with the average cell-substrate separation (h) 117 ± 6 nm, obtained by fitting the experimental data with the disk-shaped model, the values obtained from *Eqs. 25* and *19* were 38 ± 3 and 41 ± 3 nm, respectively (Table 1), which were much closer to the results measured using interference reflection microscopy (11, 27). The reason for this is that application of a disk-shaped model to VSMCs overestimated the average under-the-cell path length for current and then led to an overestimation of both the cell-substrate separation and the junctional resistance between cells when applied to measured data. We also analyzed impedance data obtained from human gingival fibroblasts and WI-38 fibroblasts ($n = 20$, Table 1). Our results show that all R_b, h, C_a, and C_b values of these two fibroblastic cell types are quite close to those of cultured VSMCs, indicating that cultured VSMCs might have a phenotype similar to fibroblasts.

Effect of RGD-containing peptide on VSMCs. ECIS was used to examine the overall cellular response from renal VSMCs when they were exposed to integrin binding peptide (GRGDSP). Figure 5 shows typical tracings of ECIS attachment data obtained from VSMC monolayers. In Fig. 5, the solid lines represent treatments with 0.5 mM GRGDSP, whereas the dotted lines represent treatments with 0.5 mM GRGESP (Gly-Arg-Gly-Glu-Ser-Pro, a control peptide that does not bind to integrins). The different color lines indicate different coatings on the electrode, as indicated. The black

Table 1. *Impedance analysis of VSMC layers from three different models and a comparison of SMCs and fibroblasts using the new model*

	R_b, Ω·cm²	h, nm	C_m, μF/cm²	C_a, μF/cm²	C_b, μF/cm²
VSMC (disk-shaped model) $r_c = 15$ mm, $a = r_c(\rho/h)^{1/2}$	0.41±0.03	117±6	2.1±0.2		
VSMC (*Eq. 25*) $W = 12$ μm, $\alpha = 0.5W(\rho/h)^{1/2}$	0.31±0.02	38±3	2.0±0.2		
VSMC (*Eq. 19*) $W = 12$ μm, $\alpha = 0.5W(\rho/h)^{1/2}$	0.32±0.02	41±3		2.6±0.1	1.7±0.1
HGF (*Eq. 19*) $W = 14$ μm, $\alpha = 0.5W(\rho/h)^{1/2}$	1.10±0.03	38±4		2.9±0.1	1.6±0.1
WI-38 fibroblast (*Eq. 19*) $W = 12$ μm, $\alpha = 0.5W(\rho/h)^{1/2}$	0.30±0.02	35±3		2.7±0.1	1.7±0.1

Values are means ± SE; $n = 42$ for vascular smooth muscle cells (VSMCs); $n = 20$ for both human gingival fibroblasts (HGF) and WI-38 fibroblasts. Using *Eq. 19* derived from the new rectangular model, we used 4 parameters to fit the measured impedance of cell-covered electrodes as a function of frequency: R_b, α, C_a, and C_b. See *Glossary* for definition of variables.

arrow indicates the time point at which the different ligands were added into the well. This was marked by a sharp transient increase in resistance in response to a small disturbance in environmental temperature due to the addition of GRGDSP or GRGESP peptide-containing solution. Regardless of different ECM protein coatings, the addition of GRGDSP lowered the resistance after the initial spike, indicating that less electrode area was covered by the VSMCs. A visual examination of the electrodes confirmed that cells contracted and rounded up after they were treated with GRGDSP, whereas addition of GRGESP peptide did not inhibit cell spreading and served as an inactive control.

The effect of varying GRGDSP concentration on the impedance of VSMC-covered electrode was monitored for 5 h. In these experiments, VSMCs were cultured on collagen I (0.2 mg/ml)-coated electrodes and became confluent monolayer 20 h after inoculation. Complete medium was used as a negative control, and hexapeptide GRGESP was used as the inactive control. At the highest concentration, 1 mM, an initial transient spike in resistance was observed almost immediately following GRGDSP addition (Fig. 6); this was followed by a drastic drop for a few hours, implying that most of the cells came loose at the end of the measurement. At 0.1 mM, the initial transient spike in resistance was similar but was followed by a slower decline. A dose-dependent relationship was generally observed, with negligible effects for the 0.01 mM concentration. Image of the electrode coverage was taken after the VSMCs were treated with 0.5 mM GRGDSP or GRGESP (Fig. 7, *top* and *bottom*, respectively). Fewer VSMCs remained attached after GRGDSP peptide treatment than after GRGESP peptide treatment. To further understand the effect of

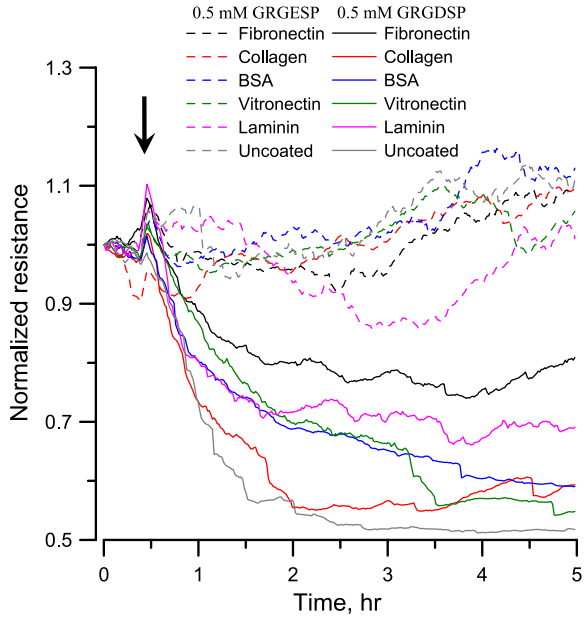

Fig. 5. Normalized resistance measured at 4 kHz showing the effect of GRGDSP and GRGESP on VSMCs grown on different extracellular matrix proteins. The different coatings used were fibronectin (black), collagen (red), BSA (blue), vitronectin (green), laminin (pink), or uncoated electrodes (gray). The same colors signify the same coatings on different electrodes. Dotted lines indicate addition of GRGESP (0.5 mM) as control, and solid lines indicate addition of GRGDSP (0.5 mM) at the moment indicated by the arrow.

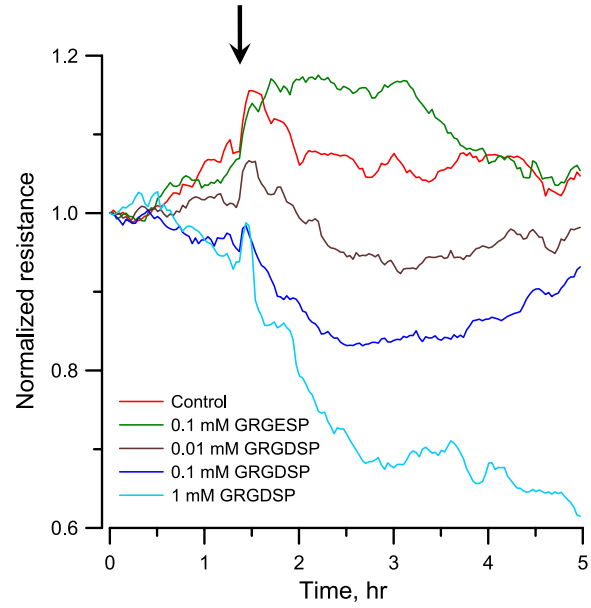

Fig. 6. Normalized resistance measurements of a confluent VSMC monolayer upon addition of different concentrations of GRGDSP. Complete medium (control; red) and GRGDSP with final concentrations of 0.01 (brown), 0.1 (dark blue), 1 (pale blue), and 0.1 mM GRGESP (green) were added to cell-covered electrode wells, and the resultant changes in normalized resistance were followed. Data were collected every 2 min for 5 h.

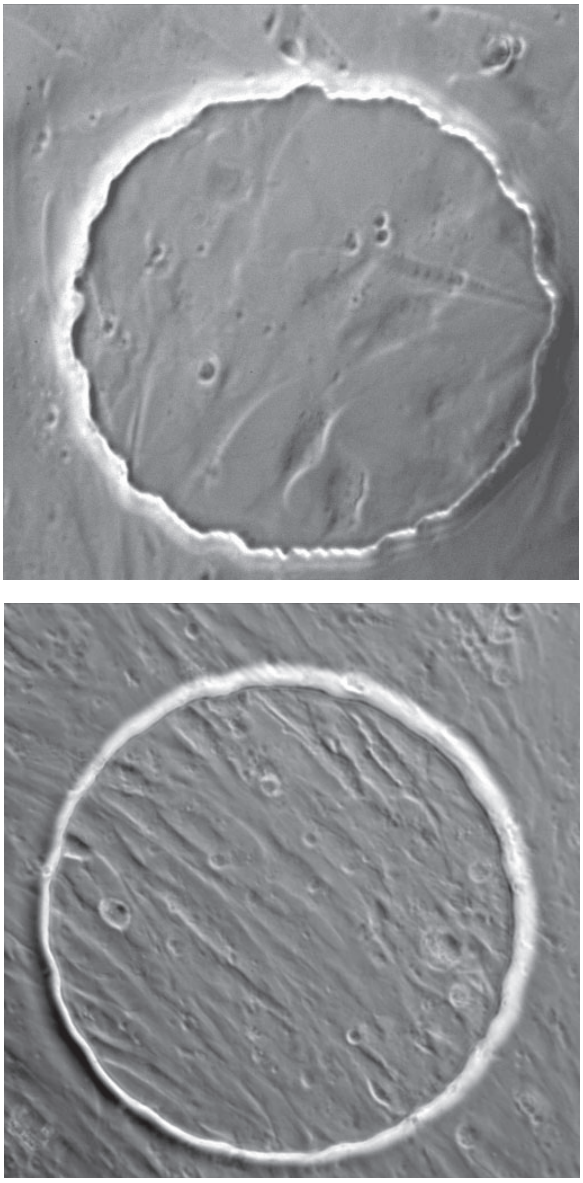

Fig. 7. Images of VSMCs on the electric cell-substrate impedance sensing (ECIS) electrode after addition of 0.5 mM GRGDSP (*top*) and 0.5 mM GRGESP (*bottom*). The gold electrode is visible as the circular area with a diameter of 250 μm.

GRGDSP addition on the changes of R_b, h, C_a, and C_b for a VSMC confluent layer, we took frequency scan measurements from cell-covered electrodes 5 h after exposure to different concentrations of GRGDSP peptide. After the data were fit with *Eq. 19*, the result indicated that upon GRGDSP challenge, the junctional resistance between cells, R_b, considerably decreased, whereas the distance between the basolateral cell surface and substratum, h, slightly increased (Table 2). Furthermore, although the basolateral membrane capacitance, C_b, stayed relatively stable, there was a dose-dependent increase in apical membrane capacitance, C_a, implying an increase of membrane folding (Table 2). In general, the specific capacitance of cell membranes is ~1 μF/cm^2 but can appear to be much larger if the membrane wrinkles. Morphological characterization using atomic force microscopy also showed that the surface roughness of VSMCs when treated with 1 mM GRGDSP was 74 ± 5 nm (n = 49), which was significantly higher than that of control cells, 45 ± 2 nm (n = 21). These observations suggest that C_a and membrane ruffling are correlated. The correlation between C_a and membrane ruffling can be validated when membrane ruffling is induced by biochemical agents or overexpression of the related signaling proteins such as RacGTPase.

Equation 19 also was used to calculate and fit time series impedance data measured from VSMC-covered electrodes upon challenge with different concentrations of GRGDSP. For example, for the time series impedance data whose resistive curves are shown in Fig. 6, both R_b and h values of each data curve were continuously traced, as shown in Fig. 8, *A* and *B*, respectively. To accomplish this, frequency scan data of each cell-covered electrode were collected before the time series impedance data were taken. Once the values of R_b, α, C_a, and C_b for each electrode had been determined through calculation of Z_c and frequency scan data fitting, these values were used as the input for the analysis of the time series data obtained from the same electrode. Whereas C_a and C_b values were kept the same to simplify the procedure of data fitting, R_b and α were used as the two variables in *Eq. 19* to calculate Z_c. After each impedance data point was fitted with the calculated values of Z_c, including both resistive and reactive components, R_b and α values over the course of the experiment were determined. Adding different concentrations of GRGDSP to the VSMCs caused a dose-dependent drop in R_b, whereas no significant effect on h (<10 nm) was observed with the addition of GRGDSP or controls, implying a relatively constant cell-substrate contact (Fig. 8). For the 1 mM GRGDSP challenge, a similar pattern between the decreased R_b value in Fig. 8*A* and the decreased normalized resistance in Fig. 6 was observed. This confirms that the decrease of R_b was mainly responsible for the decrease in measured resistance in response to GRGDSP addition. Furthermore, whereas R_b reached close to zero at *hour 5* (Fig. 8*A*), normalized resistance stayed at ~60% of control (Fig. 6), indicating that there was little cell-cell contact but relatively stable cell-substrate contact.

We also conducted time-course experiments to study the effects of GRGDSP with regard to the attachment time of the VSMCs to the substratum coated with collagen I. The measured resistance did not peak when 0.5 mM GRGDSP was added into the medium at the same time as the cells were inoculated into electrode wells (Fig. 9*A*), indicating that there was little cell attachment. When GRGDSP was added 1 h after the cells were seeded, the resistance peak was observed but was less significant than that when GRGDSP peptide was

Table 2. *Frequency scan data from confluent VSMC layers 5 h after exposure to different concentrations of GRGDSP peptide*

	R_b, Ω·cm^2	h, nm	C_a, μF/cm^2	C_b, μF/cm^2
Control	0.30±0.05	38±2	2.6±0.1	1.7±0.1
GRGESP (0.1 mM)	0.29±0.04	38±2	2.8±0.1	1.7±0.1
GRGDSP (0.01 mM)	0.25±0.03	41±2	2.8±0.1	1.6±0.1
GRGDSP (0.1 mM)	0.23±0.03	45±3	3.4±0.1	1.6±0.1
GRGDSP (1.0 mM)	0.06±0.02	45±3	3.7±0.1	1.7±0.1

Values are means ± SE (n = 4). All values R_b, h, C_a, and C_b were obtained from fitting measured impedance with *Eq. 19*.

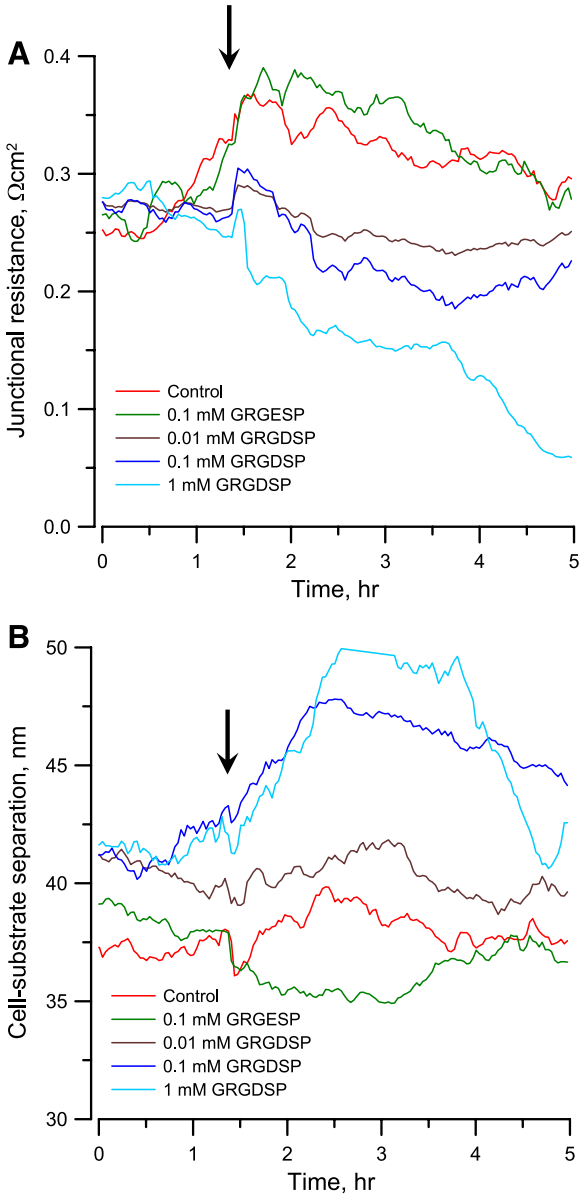

Fig. 8. Changes of junctional resistance R_b (*A*) and cell-substrate separation h (*B*) upon addition of different concentrations of GRGDSP. Complete medium (red) and GRGDSP with a final concentration of 0.01 (brown), 0.1 (dark blue), 1 (pale blue), and 0.1 mM GRGESP (green) were added. R_b and h values of each VSMC-covered electrode were traced through model calculation and data fitting of the time series impedance data whose resistive components are shown in Fig. 6. Whereas h values stayed relatively stable (<10-nm change), there was a concentration-dependent drop in R_b values.

added 3 h after seeding (Fig. 9*A*). For those experiments when GRGDSP was added over 3 h after cells were seeded (data not shown), normalized resistance curves were similar to the result in control condition without GRGDSP addition (red curve in Fig. 2), indicating no inhibition on cell attachment. A similar trend in resistance change was also observed when cell suspension was seeded in the presence of 0.5 mM GRGESP.

For cell attachment and spreading studies, if a high frequency such as 40 kHz is used, the capacitance will change in a nearly linear manner with the amount of open area on the electrode, and ECIS basically conveys information similar to that observed by a microscope (26). In our measurement at 40-kHz frequency, the single open electrode had a capacitance of ~4.2 nF (C_{open}). This was the approximate capacitance value for all the electrodes at *hour 0* when cells were inoculated into electrode wells. With a complete confluent layer of VSMCs in place, this was reduced to ~2.2 nF ($C_{confluent}$). The fraction of the electrode covered with cells is given approximately by $(C_{open} - C_{cells})/(C_{open} - C_{confluent})$ or by $[1 - (C_{cells}/C_{open})]/[1 - (C_{confluent}/C_{open})]$ if using the normalized capacitance values. In Fig. 9*B*, for example, at *hour 5*, the green curve, data obtained from the GRGDSP addition 3 h after cells were seeded, shows a partially confluent VSMC layer giving the normalized capacitance of 0.75. The fractional area covered by cells was calculated as $(1 - 0.75)/[1 - (2.2/4.2)] = 0.53$. At the 5th hour, the other three curves in Fig. 9*B*, black (GRGESP addition at *hour 0*), red (GRGDSP addi-

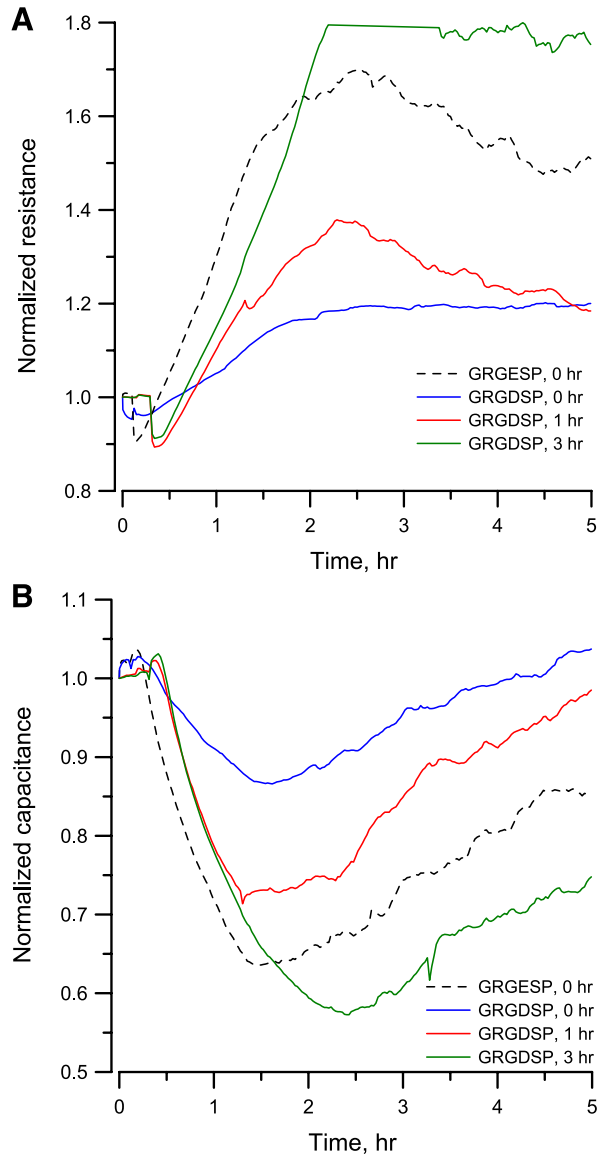

Fig. 9. Normalized resistance (*A*) and capacitance (*B*) measured at 40 kHz showing the attachment and spreading of VSMCs in response to 0.5 mM GRGDSP peptide added at different times. Solid lines represent the time-course response to the addition of GRGDSP peptide at 0 (blue), 1 (red), and 3 h (green) after inoculation of cells. Broken line indicates the time course response to the addition of 0.5 mM GRGESP peptide (black) at 0 h.

tion at *hour 1*), and blue (GRGDSP addition at *hour 0*), had normalized capacitance of 0.85, 0.95, and 1, respectively. Their fractional areas covered by cells were calculated as 0.32, 0.11, and 0, respectively.

DISCUSSION

We studied the preferential adherence and spreading of the VSMCs on different ECM coatings. The cells interact differently with various ECM proteins coated on the gold electrodes in ECIS. Although in vivo VSMCs are found in a milieu of ECM proteins, they seem to prefer collagen and fibronectin over other coatings in vitro. In general, studies using collagen or fibronectin to coat the electrodes have a quick and reliable cellular attachment (21, 26). We showed that by 2 h, the attachment of cells had peaked and cells started spreading. In the new rectangular model, the electrical potential inside the cells, V_i, was assumed to be independent of position and the transcellular current exiting from the apical membrane was uniform. The estimated capacitance of the apical membrane was slightly higher than that of the basolateral membrane based on mathematically modeling the measured impedance across cell-covered electrodes. Since the apical cell surface of an adherent cell usually has more folding than the basolateral membrane and hence displays a higher capacitance value, this new consideration is important to make model calculation agree with the experimental data as shown in Fig. 4, particularly in the high-frequency region. After renal VSMC layers are measured using frequency scan in ECIS, the calculated impedance values obtained from *Eq. 19* make an excellent fitting to the experimental data (average percentage error ~1%). The newly improved model provides a theoretical basis to interpret measured data of ECIS with regard to the morphological characteristics and cellular parameters of VSMCs in culture.

Previous studies showed that integrin binding peptide (GRGDSP) induced an increase of intracellular Ca^{2+} concentration in cultured renal VSMCs (4) and caused vasoconstriction in intact VSMCs of afferent arterioles (31). However, it is a challenge to measure contractility of cultured renal VSMCs because they are spread out in a thin monolayer, so we used ECIS to study the response of cultured VSMCs in terms of changes in cell-cell and cell-substrate interactions. Our results illustrate that irrespective of the ECM protein coating used on the electrode, the resistance drops drastically on addition of 0.5 mM GRGDSP peptide. A drop in resistance indicates that less area on the electrodes is covered by the cells, which can be due to contraction and rounding up of the cells. GRGDSP peptide-induced vasoconstriction in perfused afferent arterioles is dose dependent between 10^{-7} and 10^{-3} M (31). Using ECIS attachment experiments to follow the progressive cellular responses to GRGDSP, we found that the VSMCs responded fairly effectively to 0.1 mM GRGDSP and that 1 mM GRGDSP looked like a very strong dose, since many cells were lifting off the electrodes. Further investigations using frequency scan measurements and time series model analysis determined that the drop in impedance caused by the GRGDSP was primarily due to its effect on junctional resistance between cells, even though both the cell-substrate separation and the apical membrane capacitance increased slightly.

With the help of time-course experiments, we showed that the resistance of the electrodes during the attachment and spreading of cells did not peak in the presence of 0.5 mM GRGDSP peptide. This signifies that this peptide hinders normal formation of focal adhesion complexes by occupying integrins. On the contrary, 0.5 mM GRGESP peptide served as the control, and the peptide did not markedly affect the attachment and spreading of VSMCs. WE also noted that the effect of GRGDSP peptide in preventing cell attachment was less when added after the initial cell spreading. This peptide slightly hindered the formation of a monolayer of VSMCs when added 1 h after the inoculation of cells. However, GRGDSP peptide did not show any effect in inhibiting cell attachment when applied 3 h after the initial cell spreading. From these data, we speculate that the soluble ligand (RGD-containing peptide) binds to integrins all over the VSMCs when they are in suspension. However, once the cells have established focal adhesion, GRGDSP peptide binds more readily to the free integrins rather than replacing integrins from existing integrin-ECM complexes as shown by the lesser resistance drop in the firmly attached VSMCs. The response to GRGESP peptide at 0 h was similar to that following the addition of GRGDSP peptide after 3 h of attachment, indicating that both these ligands at the given time frame did not hinder the formation of focal adhesion, and hence the resistance of the cell-covered electrodes was higher.

The ECIS cell-electrode model, unlike other equivalent circuit models using the direct current (DC) technique, emphasizes the cell-substrate spaces and the various current paths including the current I spreading along the $\pm x$ direction in the space between ventral cell surface and the electrode surface, the current dI_i passing through the basolateral membrane, and the current dI_c from the electrode surface (Fig. 1*B*). These complex distributed currents are frequency dependent and play important roles in the measured impedance of cell-covered electrodes. For example, the ion current out of a blank electrode is perpendicular to the electrode surface. When cells cover the electrode and the cell membranes block the current, the current changes its direction to the edges of the cell through the space formed between the ventral surface of the cell and the electrode surface. Since the electric current is always from a higher potential point to a lower potential point, the electrical potential underneath the cell (V) continuously decreases from the central line ($x = 0$) of the ventral surface to the edges ($x = \pm W/2$) of the cell body. Furthermore, since dI_i and dI_c are proportional to ($V - V_i$) and ($V_c - V$), respectively, dI_i continuously decreases and dI_c continuously increases as the position moves from $x = 0$ to $x = \pm W/2$. At higher frequency this phenomenon is more substantial, and most dI_c currents are out from the electrode area close to the cell edges, causing the measured capacitive reactance to be much larger than that of a cell-free electrode. That is why at the higher frequency the capacitance of the cell-covered electrode, which is inversely proportional to the measure capacitive reactance, is much smaller than that of the cell-free electrode (Fig. 3*B*). Likewise, changes of morphological parameters such as an increase of R_b or decrease of h (i.e., increase of α) cause less current coming out of the electrode. As a result, capacitive values at higher frequencies decrease, but those at low frequencies change only little (calculation data not shown) (15, 17). It is in this general

manner that the impedance measurement and model analysis can return information regarding cell morphology.

To our knowledge, this is the first application of ECIS to characterize morphological properties of smooth muscle cell layers that display a slender and rectangular shape as most normal fibroblasts do. Although the interpretation may seem complex, it is a straightforward numerical calculation with the developed cell-electrode model. The key advantages of using *Eq. 19* (new model) rather than *Eq. 25* (previous model) for the impedance analysis of VSMC layers are providing additional information of capacitive properties of apical and basolateral membranes and improving the accuracy of fitting between the model prediction and the measured impedance data, particular in the high-frequency range. In general, the value for C_b in *Eq. 19* giving the best fit to experimental data will be somewhat smaller than the value used for C_m in *Eq. 25*, whereas C_a will be larger than C_m (Table 1). This is because using *Eq. 25* at the high frequency range underestimates the transmembrane impedance Z_m and then causes an overestimation of the transcellular current, leading to an underestimation of the spreading current under the cell and the cell-substrate separation (Table 1). The new cell-electrode model characterizes the impedance with four cellular parameters as variables. Theoretically, if a problem has n unknowns, its solution requires n equations. An impedance data point, like a complex number, contains a real part (resistance) and an imaginary part (reactance) data, and it can be used to solve two parameters using *Eq. 19*. If the frequency of the measurement is changed, the impedance characteristics of the cell-covered electrode (Z_c) will change as well. Frequency scan in ECIS measures the impedance of the cell-electrode system at multiple frequencies ranging from 25 Hz to 60 kHz, which allows good quality of the data fitting by least-squares evaluation.

Different cell types display different profiles of impedances as a function of frequency. As shown in Fig. 4*A*, for VSMCs the largest change of the measured resistance curve between cell-free and cell-covered electrodes appears at 6 kHz. This frequency is quite different from that for epithelial cells such as Madin-Darby canine kidney cells, for which the largest change is at 700 Hz (17). However, it is quite similar to fibroblastic cells such as WI-38 VA13 and HGF cells, where the largest changes are at about 4 and 6 kHz, respectively (5, 15). The frequency shift in the largest change of the measured resistance curve basically results from the changes in both α and C_a. Therefore, in the cell attachment measurement of VSMCs, we usually set the AC signal at 4 kHz (or sometimes at 40 kHz) to obtain the substantial responses of resistance (or capacitive reactance) variations to cellular activities. It is worth noting that, regarding h changes in response to 1 mM GRGDSP challenge (Fig. 8*B*), an unexpected decrease of h (i.e., increase of α) was observed over the last 1.5 h. A possible explanation is that during that period VSMCs contracted and rounded up, leading to the decrease of both R_b and h. However, according to the frequency scan data shown in Table 2, the C_a value of VSMCs 5 h after exposure to 1 mM GRGDSP peptide increased to 3.7 $\mu F/cm^2$ compared with that of the control, 2.6 $\mu F/cm^2$. Model calculation for understanding how different parameters affect the calculated impedance demonstrated a similar peak shift of normalized resistance curve resulting from increasing α or C_a. Because the attachment measurement is carried out at a single frequency, the change of C_a, unlike that of R_b and α, was not included as a variable in the fitting process of time series data. As a result, in response to 1 mM GRGDSP challenge, the impedance changes of VSMCs due to the increase of C_a might be calculated as if they were contributed from the increase of α. A continuous and speedy frequency scan measurement that allows us to calculate and fit time series impedance data with more parameters is being developed in our laboratory.

In summary, a theoretical cell-electrode model for impedance analysis of cells with slender and rectangular shape was developed and validated. Impedance analysis of VSMCs upon challenge with integrin binding hexapeptide GRGDSP was used to test the sensitivity of the model. The model was able to detect changes in the junctional resistance, the average distance between the ventral cell surface and substratum, and capacitance values of apical and basolateral cell membranes. The model provides a theoretical basis to interpret measured data of ECIS regarding to the morphological characteristics and cellular parameters of cells in culture. Because of the simplicity of the system, impedance analysis of cells layers measured by ECIS will find more applications in biological research.

ACKNOWLEDGMENTS

We acknowledge Daniel Opp for technical assistance.

GRANTS

This work was supported by National Institutes of Health Grants 1R03 CA123621-01A1 (C.-M. Lo) and DK-60501 (K.-P. Yip), a Predoctoral Fellowship (L. Balasubramanian), and a Grant-In-Aid (K.-P. Yip) from the American Heart Association, Florida/Puerto Rico Affiliate.

REFERENCES

1. **Atienza JM, Yu NC, Kirstein SL, Xi B, Wang XB, Xu X, Abassi YA.** Dynamic and label-free cell-based assays using the real-time cell electronic sensing system. *Assay Drug Dev Technol* 4: 597–607, 2006.
2. **Atienza JM, Zhu J, Wang XB, Xu X, Abassi Y.** Dynamic monitoring of cell adhesion and spreading on microelectronic sensor arrays. *J Biomol Screen* 10: 795–805, 2005.
3. **Bodmer JE, English A, Brady M, Blackwell K, Haxhinasto K, Fotedar S, Borgman K, Bai EW, Moy AB.** Modeling error and stability of endothelial cytoskeletal membrane parameters based on modeling transendothelial impedance as resistor and capacitor in series. *Am J Physiol Cell Physiol* 289: C735–C747, 2005.
4. **Chan WL, Holstein-Rathlou NH, Yip KP.** Integrin mobilizes intracellular Ca^{2+} in renal vascular smooth muscle cells. *Am J Physiol Cell Physiol* 280: C593–C603, 2001.
5. **Giaever I, Keese CR.** Micromotion of mammalian cells measured electrically. *Proc Natl Acad Sci USA* 88: 7896–7900, 1991. [Erratum. *Proc Natl Acad Sci USA* 90 (Feb): 1634, 1993.]
6. **Giaever I, Keese CR.** Monitoring fibroblast behavior in tissue culture with an applied electric field. *Proc Natl Acad Sci USA* 81: 3761–3764, 1984.
7. **Giaever I, Keese CR.** A morphological biosensor for mammalian cells. *Nature* 366: 591–592, 1993.
8. **Giaever I, Keese CR.** Use of electric fields to monitor the dynamical aspect of cell behavior in tissue culture. *IEEE Trans Biomed Eng* 33: 242–247, 1986.
9. **Gordienko DV, Clausen C, Goligorsky MS.** Ionic currents and endothelin signaling in smooth muscle cells from rat renal resistance arteries. *Am J Physiol Renal Fluid Electrolyte Physiol* 266: F325–F341, 1994.
10. **Hedin U, Bottger BA, Luthman J, Johansson S, Thyberg J.** A substrate of the cell-attachment sequence of fibronectin (Arg-Gly-Asp-Ser) is sufficient to promote transition of arterial smooth muscle cells from a contractile to a synthetic phenotype. *Dev Biol* 133: 489–501, 1989.
11. **Izzard CS, Lochner LR.** Formation of cell-to-substrate contacts during fibroblast motility: an interference-reflexion study. *J Cell Sci* 42: 81–116, 1980.

12. **Keese CR, Karra N, Dillon B, Goldberg AM, Giaever I.** Cell-substratum interactions as a predictor of cytotoxicity. *In Vitr Mol Toxicol* 11: 183–192, 1998.
13. **Ko KSC, Lo CM, Ferrier J, Hannam P, Tamura M, McBride BC, Ellen RP.** Cell-substrate impedance analysis of epithelial cell shape and micromotion upon challenge with bacterial proteins that perturb extracellular matrix and cytoskeleton. *J Microbiol Methods* 34: 125–132, 1998.
14. **Kowolenko M, Keese CR, Lawrence DA, Giaever I.** Measurement of macrophage adherence and spreading with weak electric fields. *J Immunol Methods* 127: 71–77, 1990.
15. **Lo CM, Ferrier J.** Impedance analysis of fibroblastic cell layers measured by electric cell-substrate impedance sensing. *Phys Rev E Stat Phys Plasma Fluids Relat Interdiscip Topics* 57: 6982–6987, 1998.
16. **Lo CM, Glogauer M, Rossi M, Ferrier J.** Cell-substrate separation: effect of applied force and temperature. *Eur Biophys J* 27: 9–17, 1998.
17. **Lo CM, Keese CR, Giaever I.** Impedance analysis of MDCK cells measured by electric cell-substrate impedance sensing. *Biophys J* 69: 2800–2807, 1995.
18. **Lo CM, Keese CR, Giaever I.** Monitoring motion of confluent cells in tissue culture. *Exp Cell Res* 204: 102–109, 1993.
19. **Lo CM, Keese CR, Giaever I.** pH changes in pulsed CO_2 incubators cause periodic changes in cell morphology. *Exp Cell Res* 213: 391–397, 1994.
20. **Naito M, Funaki C, Hayashi T, Yamada K, Asai K, Yoshimine N, Kuzuya F.** Substrate-bound fibrinogen, fibrin and other cell attachment-promoting proteins as a scaffold for cultured vascular smooth muscle cells. *Atherosclerosis* 96: 227–234, 1992.
21. **Salas PJ, Vega-Salas DE, Rodriguez-Boulan E.** Collagen receptors mediate early events in the attachment of epithelial (MDCK) cells. *J Membr Biol* 98: 223–236, 1987.
22. **Schwan HP.** Linear and nonlinear electrode polarization and biological materials. *Ann Biomed Eng* 20: 269–288, 1992.
23. **Slaughter GE, Bieberich E, Wnek GE, Wynne KJ, Guiseppi-Elei A.** Improving neuron-to-electrode surface attachment via alkanethiol self-assembly: an alternating current impedance study. *Langmuir* 20: 7189–7200, 2004.
24. **Smith TJ, Wang HS, Hogg MG, Henrikson RC, Keese CR, Giaever I.** Prostaglandin E_2 elicits a morphological change in cultured orbital fibroblasts from patients with graves ophthalmopathy. *Proc Natl Acad Sci USA* 91: 5094–5098, 1994.
25. **Warburg E.** Polarization capacity of platinum. *Ann Phys* 6: 125–135, 1901.
26. **Wegener J, Keese CR, Giaever I.** Electric cell-substrate impedance sensing (ECIS) as a noninvasive means to monitor the kinetics of cell spreading to artificial surfaces. *Exp Cell Res* 259: 158–166, 2000.
27. **Woods A, Couchman JR.** Protein kinase C involvement in focal adhesion formation. *J Cell Sci* 101: 277–290, 1992.
28. **Xiao C, Luong JHT.** Assessment of cytotoxicity by emerging impedance spectroscopy. *Toxicol Appl Pharmacol* 206: 102–112, 2005.
29. **Xiao C, Luong JHT.** On-line monitoring of cell growth and cytotoxicity using electric cell-substrate impedance sensing (ECIS). *Biotechnol Progr* 19: 1000–1005, 2003.
30. **Yamamoto K, Yamamoto M.** Cell adhesion receptors for native and denatured type I collagens and fibronectin in rabbit arterial smooth muscle cells in culture. *Exp Cell Res* 214: 258–263, 1994.
31. **Yip KP, Marsh DJ.** An Arg-Gly-Asp peptide stimulates constriction in rat afferent arteriole. *Am J Physiol Renal Physiol* 273: F768–F776, 1997.
32. **Yu NC, Atienza JM, Bernard J, Blanc S, Zhu J, Wang XB, Xu X, Abassi YA.** Real-time monitoring of morphological changes in living cells by electronic cell sensor arrays: an approach to study G protein-coupled receptors. *Anal Chem* 78: 35–43, 2006.